

Knudsen Effect on the Estimation of the Effective Thermal Conductivity of Thermal Barrier Coatings

J.H. Qiao, R. Bolot, H.L. Liao, and C. Coddet

(Submitted July 2, 2012; in revised form November 22, 2012)

A numerical model based on the use of cross-sectional micrographies and a 3D image of thermal barrier coatings for the estimation of the material effective thermal conductivity is presented. The case of a YSZ thermal spray coating consisting of a 2 phase network, namely, the coating material and pores, is considered. The variation of the thermal conductivity of pores caused by their small size was considered by taking the Knudsen effect into account. The quantification of this effect on the effective thermal conductivity of the coating was achieved with the help of image analysis combined with an in-house program coded in C language. Finite-difference (FD) and finite-element (FE) models were applied using both 2D images and a 3D image. Despite the differences in the computed values obtained with these two numerical methods, the decrease of the computed thermal conductivity caused by the Knudsen effect was found to remain quite moderate for both methods (i.e., about 3-5% for the 3D results).

Keywords 2D and 3D, Knudsen effect, numerical modeling, thermal barrier coatings, thermal conductivity

1. Introduction

The performances of ceramics are affected by various factors, among which the microstructure may be the most important, and is the most complex one. Efforts have been intensively devoted to identify the relationships between the microstructure and resulting effective properties of ceramics. Different analytical models were put forward to solve this problem, such as the Maxwell (Ref 1) and Bruggeman models (Ref 2). Hasselman proposed a simple model accounting for the effect of cracks on thermal conductivity (Ref 3). This approach was also followed by Sevostianov and Kachanov (Ref 4, 5). Litovsky et al. (Ref 6, 7) suggested a fractal model to represent ceramic and refractory materials. In their studies, it is worth mentioning that the effective thermal conductivity of the gas trapped within the pores is influenced not only by the

temperature and pressure, but also by the dimension of the pores at the micro scale level by complying with a deduced equation (Ref 8). This effect depends upon the Knudsen number, and is called Knudsen effect or rarefaction effect. Especially for submicron or nanoscaled pores, the decrease in the thermal conductivity of the trapped gas appears obvious. In practice, thermal barrier coatings (TBCs) present a structure containing mainly such kinds of pores and cracks. Therefore, many efforts (Ref 9, 10) were devoted to estimate the Knudsen effect on the thermal conductivity of TBCs with some analytical models. In these models, the dimension of a type of pore was assumed to be uniform so that the applied gas conductivity can not be fully reliable.

More recently, models were also directly developed from microstructural images with the help of image analysis (IA) (Ref 11, 12) to describe the real microstructure of the materials. This type of modeling is called image-based modeling and was intensively applied for TBCs. Several studies have taken advantage of using finite-element (FE) software tools, such as OOF (Ref 13, 14) and ANSYS (Ref 15), to estimate the effective elastic modulus (Ref 16-18) and thermal conductivity of coatings from 2D cross-sectional images (Ref 19, 20) and 3D images captured by x-ray tomography techniques (Ref 21-23) or generated with an image morphing method from 2D images (Ref 24, 25). An alternative approach was developed at UTBM and consists in the use of a finite difference method (FDM) to solve the numerical problem with an in-house code named TS2C (Ref 26-28). However, the Knudsen effect on the thermal conductivity of TBCs was quite difficult to quantify for image-based modeling because of the variable dimensions of each pore.

This study aimed at combining IA and a FD model for quantifying the Knudsen effect on the thermal

This article is an invited paper selected from presentations at the 2012 International Thermal Spray Conference and has been expanded from the original presentation. It is simultaneously published in *Thermal Spray 2012: Proceedings of the International Thermal Spray Conference, Air, Land, Water, and the Human Body: Thermal Spray Science and Applications*, Houston, Texas, USA, May 21-24, 2012, Basil R. Marple, Arvind Agarwal, Laura Filofteia-Toma, Margaret M. Hyland, Yuk-Chiu Lau, Chang-Jiu Li, Rogerio S. Lima, and André McDonald, Ed., ASM International, Materials Park, OH, 2012.

J.H. Qiao, R. Bolot, H.L. Liao, and C. Coddet, IRTES-LERMP/UTBM, Belfort, France. Contact e-mail: jianghao.qiao@utbm.fr.

conductivity of TBCs. The dimensions of every pore were measured using an image processing software and by applying an in-house numerical algorithm. The size-induced decrease of the gas thermal conductivity was thus determined for all pixels in the pores. Finally, the Knudsen effect on the thermal conductivity of TBCs was computed by both 2D and 3D models developed from cross-sectional images and a 3D artificial coating image reconstructed from 2D images with IA, respectively. Additionally, FE computations were also implemented for the same images for comparison.

2. Typical Structure of YPSZ Coatings

The coatings were elaborated by atmospheric plasma spraying of a SULZER-METCO 7 wt.% yttria partially stabilized zirconia (YPSZ) powder. Polished cross sections of the coatings were observed with scanning electron microscopy (SEM). However, calculation results depend, on the resolution of the coating SEM, which reproduce more or less faithfully the pore architecture of the coating. Backscattering electron mode was chosen by virtue of a very sharp contrast between the YPSZ matrix and the pores. Images were captured in the format 1024×768 pixels with a corresponding resolution of $0.14 \mu\text{m}/\text{pixel}$. Figure 1 presents a typical cross-sectional micrograph. The porosity of the coating determined by image analysis for six images (Ref 28) was $19.0 \pm 1.1\%$.

3. Numerical Computation

The numerical models were developed directly from the coating cross-sectional micrographies using the FEM and the FDM (Ref 27): each pixel of the image corresponds to an element in FEM-based model or a cell in FDM-based model. Figure 2 presents a schematic view of a 2D model generated from a binary image obtained by applying an adequate threshold (Ref 28), in which the thermal properties were assigned to each pixel versus its

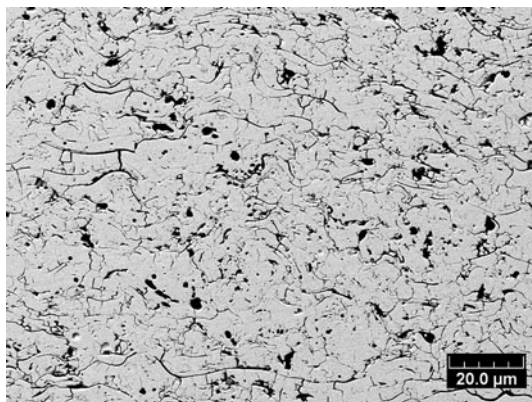


Fig. 1 Example of cross-sectional micrograph of plasma sprayed Y-PSZ coating

color: white pixels are assigned to YPSZ and the black ones to pores. Additionally, the conductivities of pores were determined with regard to the Knudsen effect. After solving the problem, the effective thermal conductivity (λ_{eff}) corresponding to the image was calculated from an equation correlating it to the thermal flux and temperature gradient across the domain, as follows:

$$\lambda_{\text{eff}} = \frac{\Phi L}{W \Delta T} \quad (\text{Eq 1})$$

in which Φ represents the thermal flux; ΔT is the temperature difference across the domain such as on Fig. 2; W and L are the width and height of the domain respectively.

Figure 3 shows a schema of the 3D model. This model was built from a 3D artificial image, and one voxel corresponds to a cubic element. This 3D image was previously reconstructed from the microstructural information of the pore network obtained by IA from 2D images (Ref 29). The porosity was classified into three types (interlamellar, intrasplat, and globular pores (Ref 30)) and then separately quantified for the 2D images. These types were, individually, regenerated into the 3D YPSZ matrix to form a representative image according to their dimensions, orientations, morphologies, and porosity rate. Considering the computational capability of the available PC, the 3D image was represented with a size of $300 \times 300 \times 300$ voxels.

4. Thermal Conductivity and Knudsen Effect

The microstructure of the YPSZ phase was considered to be uniform so that the thermal conductivity of the 7 wt.% YPSZ material (λ_m) was chosen as $2.5 \text{ W/m}\cdot\text{K}$ (Ref 19). Regarding the pores, the conductivity (λ_g) can be estimated as the thermal conductivity of air trapped in pores as first approximation. However, since the mean free path of air molecules may be of the same order as the

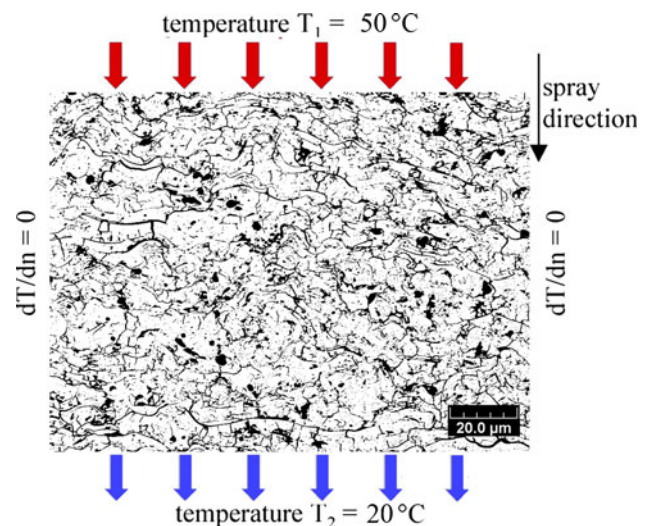


Fig. 2 Schematic view of a 2D problem

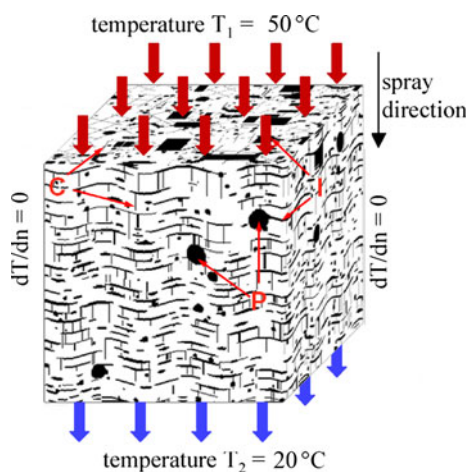


Fig. 3 Schematic view of a 3D problem. In the image, the symbol “I” points to the interlamellar pores; “C” to the intra-splat cracks; and “P” to the globular pores

pore thickness, the effective thermal conductivity of pores can differ significantly from that of air in an unconfined environment because of the Knudsen effect (i.e., rarefaction effect). Consequently, for a gas layer, it can be expressed alternatively as (Ref 6, 7, 9, 10):

$$\lambda_g = \lambda_{\text{atm}} \frac{1}{1 + C \left(\frac{T}{p\delta} \right)} \quad (\text{Eq 2})$$

where λ_{atm} is the gas conductivity at atmospheric pressure (0.025 W/m·K); p is the gas pressure in a crack gap; δ is the thickness of a crack and the coefficient $C = 2.5 \times 10^{-5} \text{ Pa/m}\cdot\text{K}$ for air (Ref 7). Although the thermal conductivity of air within a spherical pore is certainly slightly smaller than λ_{atm} according to Eq 2 (Ref 9), most of the spherical pores are so large that the Knudsen effect can be ignored.

Owing to negligible temperature change (from 20 to 50 °C) and to negligible temperature-induced changes of the gas pressure, constant values of 300 K and 1 atm were applied in Eq 2. The value of λ_g tends thus to decrease with the decrease of the crack dimension, as shown in Fig. 4. The maximum value of λ_g is equal to the thermal conductivity of air in an unconfined atmosphere (0.025 W/m·K). The value of λ_g is 5% lower for a 1.4- μm thick pore (~10 pixels in the 1000-time magnified images). However, for the thinnest observable pores (1 pixel), the value of λ_g decreases down to 0.016 W/m·K. In the following studies, the thickness of the cracks will be determined by means of IA.

5. Measurement of the Crack Thickness by Image Analysis

Although λ_g may be significantly influenced by the crack thickness, no report taking the Knudsen effect into account could be found for coatings, maybe because of

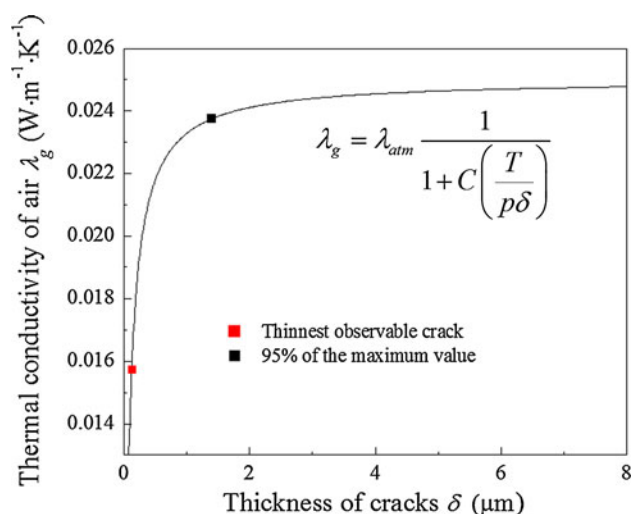


Fig. 4 Influence of the thickness of the crack gaps on the thermal conductivity of air

difficulties to know the thickness of the crack gaps. Fortunately, IA allowed us to measure approximately the thickness for each crack gap. In particular, images were analyzed by combining the use of Scion image package (Beta Release 4), followed by treatments and analysis by a new algorithm.

The detailed process is described as follows: Images, such as that shown in Fig. 1, are first converted to a binary image by applying an adequate threshold (Ref 28) (Fig. 5a). Second, the micro pore network is obtained after subtracting the pores presenting a diameter or thickness no smaller than 10 pixels (i.e., 1.4 μm) from the original image by implementing “2D rolling ball” operation (Fig. 5b). The subtracted pores are globular and play a smaller role in the decrease of heat transfers in comparison with interlamellar pores. Thus, the change of λ_g was ignored for them. Third, the micro pore skeleton (represented by red pixels in Fig. 5c and d) with a thickness of 1 pixel was obtained by implementing a “skeletonization” operation. Fourth, the skeleton within each pixel is assumed to be straight. Thus, it presents a unique angle (versus X axis) which could be approximately determined by the orientations of its neighbors versus itself. The angle (0-90°) was thus recorded in an array $\text{Angle}[nx][ny]$ in which the values are null for pixels without skeleton. Examples of 45° and 22.5° are illustrated in Fig. 5(d), and the rest can be done in the same manner. Finally, the orientation of the skeleton can be regarded as that of the crack. Therefore, the angles were assigned to the “flesh” (i.e., the black pixels in Fig. 5d) of the crack perpendicularly to the crack orientation. Meanwhile, all red and black pixels in the normal (perpendicular) direction are counted for measuring the thickness of the crack. For finding them in a convenient and simple method, the values of the angles and thicknesses were recorded at the corresponding coordinate positions in arrays $\text{Angle}[nx][ny]$ and $\text{Thic}[nx][ny]$, respectively.

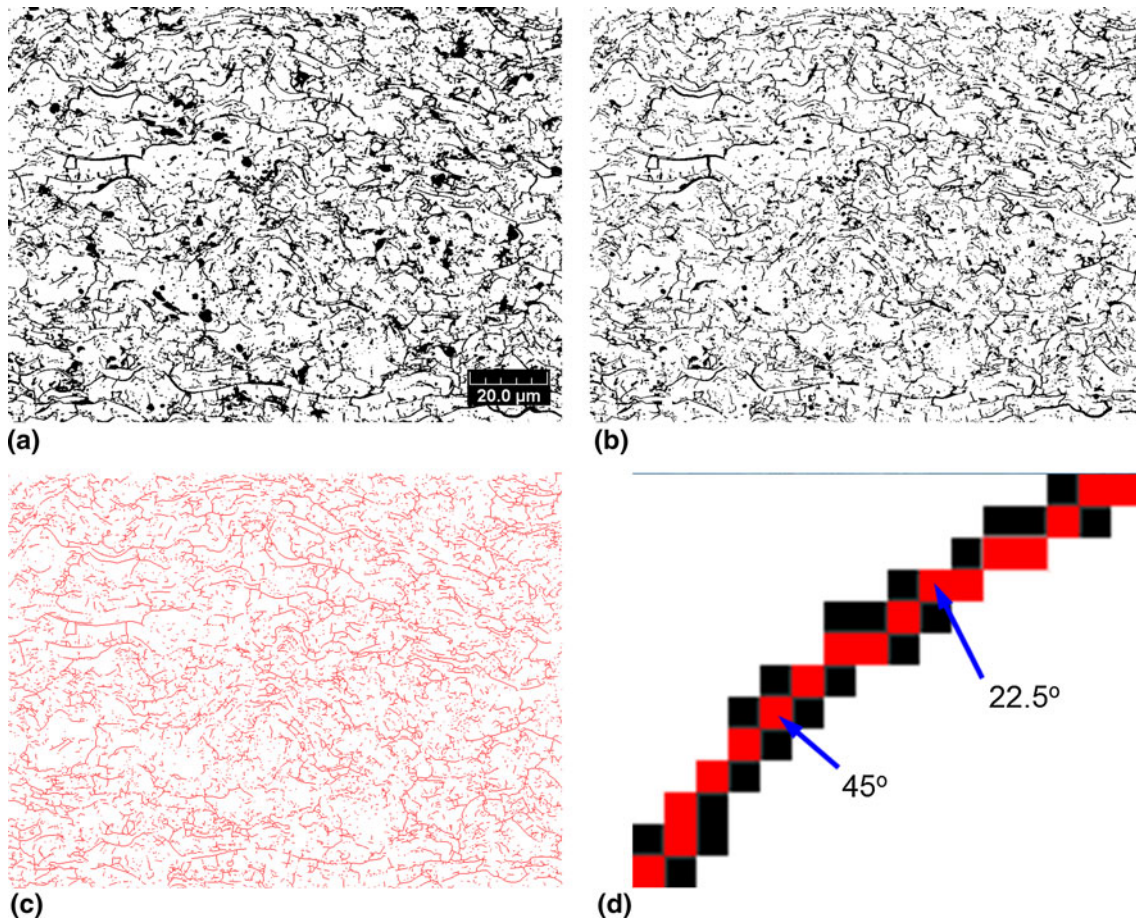


Fig. 5 Measurement process of the pore thickness by image analysis for pores smaller or thinner than $1.4 \mu\text{m}$ to apply the Knudsen effect. (a) Thresholding; (b) micro pores; (c) skeleton; and (d) detail of a pore

6. Numerical Results and Analysis

6.1 Knudsen Effect on the Thermal Conductivity of Pores in Coatings

In view of its negligible influence for large pores, the Knudsen effect was taken into account only for pores with a dimension lower than or equal to $1.4 \mu\text{m}$. Thus, a value of $0.025 \text{ W/m}\cdot\text{K}$ was directly assigned to the largest pores. Figure 6 shows the thermal conductivity field for pores considering the Knudsen effect. A high conductivity is represented by light blue and a low one by dark blue, in the range $0.016\text{--}0.025 \text{ W/m}\cdot\text{K}$. The solid material is white. It can be obviously observed that a lowering of the thermal conductivity arises in thin pores. It mainly confirmed that the thinner the pores are, the lower the thermal conductivity is. Furthermore, about 81% of the pores (versus total porosity) present a thermal conductivity below $0.024 \text{ W/m}\cdot\text{K}$. However, only a small fraction of them presents a thermal conductivity close to the lower value: about 30% below $0.020 \text{ W/m}\cdot\text{K}$ and 5% only equal to $0.016 \text{ W/m}\cdot\text{K}$.

6.2 Improvement for the Pores Smaller Than a Pixel

Owing to the existence of pores smaller than a pixel, a direct measurement seems not applicable for them. Fortunately, their conductance could be estimated by combining a model to the Knudsen effect.

In practice, a majority of the pixels containing both pores and solid material will be overestimated and set as pores after the threshold application. For thick pores, the effect of the increase in their thickness is thus negligible. However, for the thinnest pores, the increase in thickness has to be taken into account. On the other hand, the maximum temperature gradient is proved to be perpendicular to the orientation of the cracks. Therefore, the thermal conductivity in the direction perpendicular to the temperature gradient may be inessential because that in the parallel direction seems much more important to influence the thermal resistance.

A model is proposed to illustrate the effective thermal conductivity of a pixel. In the direction of the temperature gradient, the pores and the solid material are considered

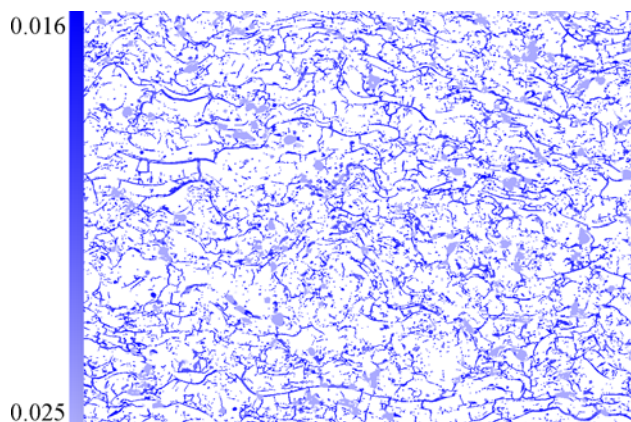


Fig. 6 Field of thermal conductivity of pores determined by the Knudsen law

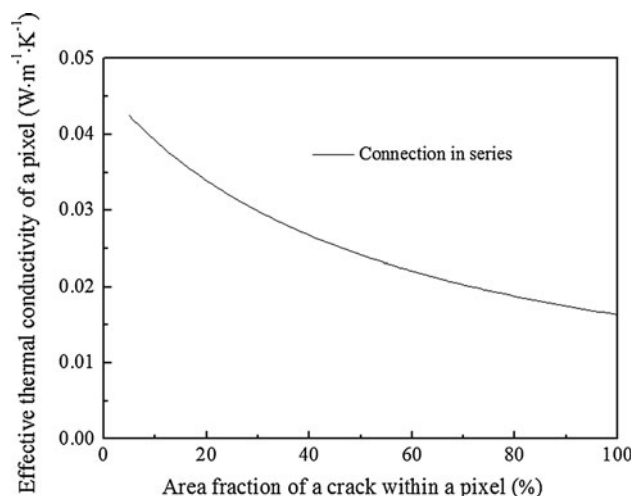


Fig. 7 Effective thermal conductivity of a pixel vs. crack area fraction for pores smaller than $0.14 \mu\text{m}$

to connect in series, and the effective thermal conductivity can be expressed as

$$\lambda_c = \frac{1}{(1 - f_p)/\lambda_m + f_p/\lambda_g} \quad (\text{Eq 3})$$

The thickness fraction of pores is equal to the volume fraction (f_p) by assuming a parallelogram pore within a pixel. λ_g is substituted from Eq 2 so that the following equation is derived:

$$\lambda_c = \frac{\delta_0}{\frac{\delta_0 - \delta}{\lambda_m} + \frac{p\delta + CT}{p\lambda_{\text{atm}}}} \quad (\text{Eq 4})$$

in which $\delta_0 = 0.14 \mu\text{m}$. Thus, the influence of the pore thickness on the effective thermal conductivity of a pixel is presented in Fig. 7.

With the reduction of the thickness of pores, the decrease in thermal conductivity due to the Knudsen effect nullifies the decrease in the volume fraction of pores. As a

result, an evident decrease could not be observed when the thickness of pores increases. In fact, pixels with a low fraction of pores will be converted to white (solid material) so that the right part is more significant. Consequently, the value $0.016 \text{ W/m}\cdot\text{K}$ was presently used for all pores smaller than a pixel.

6.3 Knudsen Effect on the Computed Thermal Conductivity of Coatings

The Knudsen effect on the thermal conductivity of coatings was first demonstrated by comparisons between 2D computations with the FDM. Six cross-sectional images were used to obtain a reliable value. The average results and standard deviation are shown in Table 1. As a result, the computed thermal conductivity was $0.59 \pm 0.02 \text{ W/m}\cdot\text{K}$ with the previous method (Ref 28). As a comparison, it decreases to $0.54 \pm 0.03 \text{ W/m}\cdot\text{K}$ by considering the Knudsen effect (shown in Table 1). The difference between them is thus less than 8%, and seems much smaller than the expected value. It must be explained that extremely fine pores (i.e., smaller than $0.14 \mu\text{m}$) could not be characterized with the present image resolution. These pores were either broadened to 1 pixel or partially lost by the binarization of the image. Thus, the Knudsen effect was weakened in the actual computations. Moreover, the porosity is only about 19%, and the proportion of thin pores is relatively low for the present coatings. Nevertheless, the application of this study is still suggested for porous structures, especially those containing thin pores.

3D images can be generated by sophisticated technologies, such as x-ray tomography (Ref 21-23) and serial sectioning (Ref 31, 32). However, these techniques are limited in terms of resolution ($> 1 \mu\text{m}/\text{voxel}$) for capturing the features of thin cracks. Alternatively, a 3D numerical model was developed from an artificial coating image generated by using information obtained for a real coating microstructure as shown in Fig. 3. In view of the differences between 2D and 3D computations (Ref 24, 25, 29, 33), the modeling was implemented to manifest the Knudsen effect for both cases. 2D computations were also performed for each cross section of the 3D artificial image (including the 300 ones parallel to the X-Y plane and the 300 ones parallel to the Y-Z plane). In the 2D case, the Knudsen effect caused a decrease of the calculated average thermal conductivity from 0.61 to $0.56 \text{ W/m}\cdot\text{K}$ (shown in Table 1), which is almost equal to the effect corresponding to the real images (8% and $0.05 \text{ W/m}\cdot\text{K}$). However, for the 3D computation, the Knudsen effect seems smaller, causing a decrease of only about 3%, (from 0.95 to $0.92 \text{ W/m}\cdot\text{K}$).

The heat-transfer mechanism may be understood in a simple manner: the heat flow tries to find an optimized way to bypass the pores through the structure. However, a part of the heat flow cannot find a better way than flowing through the pore network. For the 3D modeling, this part is lower because the heat flow may have an alternative way in the third dimension. Consequently, the change of λ_g is less sensitive on the computed results in the 3D model.

Table 1 Thermal conductivities of coatings computed by taking or without taking the Knudsen effect into account with 2D and 3D FDM modeling

Image type	Effective thermal conductivity, W/m·K		Knudsen effect, %
	Without Knudsen	With Knudsen	
2D images	0.59 ± 0.02	0.54 ± 0.03	8
2D cross sections of the 3D image	0.61 ± 0.00	0.56 ± 0.00	8
3D image	0.95	0.92	3

Table 2 Thermal conductivities of coatings computed by taking or without taking the Knudsen effect into account with 2D and 3D FEM-based modeling

Image type	Effective thermal conductivity, W/m·K		Knudsen effect, %
	Without Knudsen	With Knudsen	
2D images	0.71 ± 0.02	0.67 ± 0.03	6
2D cross sections of the 3D image	0.76 ± 0.02	0.71 ± 0.02	7
3D image	1.17 ± 0.02	1.12 ± 0.03	4

6.4 Validation for FEM-based Modeling

The Knudsen effect on the thermal conductivity of coatings was estimated for FDM-based modeling. Some complementary investigations were, however, implemented using FEM-based modeling in view of the differences between FEM- and FDM-based models (Ref 34). In particular, ANSYS was used for performing both 2D and 3D computations using the above mentioned images. Because of the higher consumption of RAM for ANSYS, the 3D image had to be segmented with a dimension of $150 \times 150 \times 150$ voxels for each part (eight distinct volumes in the $300 \times 300 \times 300$ voxels initial structure). The results were then averaged and are shown in Table 2.

Similar to the case of the FDM-based model, the decrease of the thermal conductivity was confirmed by the FEM computations for both the real images and the 3D artificial coating image. The 2D-computed thermal conductivity decreases from 0.71 ± 0.02 to 0.67 ± 0.03 W/m·K, by about 6%, for the real images, and from 0.76 ± 0.02 to 0.71 ± 0.02 W/m·K, by about 7%, for the cross sections of the 3D artificial coating image. For the 3D computations, the Knudsen effect is also slightly smaller, causing a decrease of only about 4%, from 1.17 ± 0.02 to 1.12 ± 0.03 W/m·K. These reductions are not very different in comparison with values obtained from FDM-based modeling (8 and 3% for the 2D and 3D cases, respectively).

However, the difference between 2D and 3D computations are relatively large. In the 2D model, each pixel exchanges heat with its neighbours in the plane so that the heat

flow perpendicular to the section is not taken into account. In the 3D model, a new path is supplied for the heat transfer around the pores in the third dimension. Therefore, the obstructive action of pores is weakened, compared with the 2D case. For this reason, the 3D-computed thermal conductivity is higher than the 2D values. Thus, the use of 3D modeling is strongly recommended for TBCs, and the results are closer to the experimental value of 0.99 W/m·K for this coating (Ref 35).

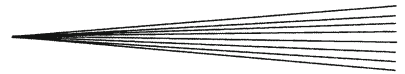
It may also be noticed that the thermal conductivities computed with FEM-based modeling are higher than those obtained with our code based on FDM. The differences concerning 3D modeling (21-23%) are very close to those of 2D modeling (24-27% for the same artificial structure, although a smaller domain had to be considered with ANSYS (due to higher memory requirements).

The major reason, demonstrated elsewhere (Ref 28), is the different discretization methods for the two models: a cell-centered formulation is used in our code, whereas a nodal formulation is applied in FEM-based models. The different formulations lead to different expressions of the thermal resistances between cells or nodes: in-series for the former and in-parallel for the latter. The second reason concerns the different interpolation functions applied for the two methods. Nevertheless, the Knudsen effect is quite similar for both numerical methods. Therefore, it can be stressed that the quantification of the Knudsen effect with both methods is reliable.

7. Conclusions and Perspectives

The quantification of the Knudsen effect on heat transfer through a porous structure was first realized by image-based numerical modeling using FD and FE methods in the present study. The pore thicknesses in any location of the treated images were determined by IA so that the Knudsen effect on the gas conduction in the pores (both globular pores and cracks) could be quantified. The influence of the pore dimension on the computed results was estimated for pores thinner than one pixel. As a result, the computed thermal conductivity field of pores shows a relatively good accordance with the expected one.

However, only small changes were noticed on the computed average thermal conductivity of plasma sprayed Y-PSZ coatings while taking the Knudsen effect into account. In particular, the effective thermal conductivity was found to decrease by 8% (difference of 0.05 W/m·K), for the 2D model and by 3% (0.03 W/m·K) for the 3D model. Results obtained with the FDM-based model were also compared with those produced with a FEM-based modeling implemented within ANSYS. For the FEM-based model, the computed thermal conductivity was found to decrease by 6-7% (0.04 - 0.05 W/m·K) for the 2D case and by 4% (0.05 W/m·K) for the 3D case. The main reason is that the porosity level of very thin pores is relatively low (about 1% for the 0.14 - μm thick pores). The other reason is that the minimum thermal conductivity corresponding to a one-pixel thick pore (0.014 μm) is 0.016 W/m·K,



which corresponds to a reduction of only 36% in comparison with the original value of 0.025 W/m·K. Therefore, if a much higher resolution of images is chosen, the Knudsen effect could be more obvious. However, the representativeness of the captured zone must be considered first of all.

Compared with results obtained with the FE method, the resulting thermal conductivities calculated with the FD method are smaller for both 2D and 3D models, by 24-27 and 21-23%, respectively. However, the similar reduction of computed thermal conductivity for both numerical methods confirmed the reliability of the quantification of the Knudsen effect. Therefore, it can be stressed that the Knudsen effect is 6-8% for 2D modeling and 3-4% for 3D modeling.

The method for quantifying the Knudsen effect and predicting the effective properties of thermal sprayed coatings will be further improved for high temperature conditions by considering the thermomechanical coupling. Some modeling studies of thermal expansion and stress, such as (Ref 17), will be completed, and the corresponding change of morphology of the coatings could be simulated. Furthermore, this study could also be implemented for the actual service temperature of coatings.

References

1. J. Maxwell, *A Treatise on Electricity and Magnetism*, Clarendon Press, Oxford, 1873
2. D.A.G. Bruggeman, Berechnung Verschiedener Physikalischer Konstanten von Heterogenen Substanzen, *Ann. Physik*, 1935, **24**, p 636 (in German)
3. D.P.H. Hasselman, Effect of Cracks on Thermal-Conductivity, *J. Compos. Mater.*, 1978, **12**, p 403-407
4. I. Sevostianov and M. Kachanov, Plasma-Sprayed Ceramic Coatings: Anisotropic Elastic and Conductive Properties in Relation to the Microstructure; Cross-Property Correlations, *Mater. Sci. Eng. A*, 2001, **297**, p 235-243
5. B. Shafiro and M. Kachanov, Anisotropic Effective Conductivity of Materials with Nonrandomly Oriented Inclusions of Diverse Ellipsoidal Shapes, *J. Appl. Phys.*, 2000, **87**, p 8561-8569
6. E.Y. Litovsky and M. Shapiro, Gas Pressure and Temperature Dependences of Thermal Conductivity of Porous Ceramic Materials: 1. Refractories and Ceramics with Porosity Below 30-Percent, *J. Am. Ceram. Soc.*, 1992, **75**, p 3425-3439
7. E.Y. Litovsky, M. Shapiro, and A. Shavit, Gas Pressure and Temperature Dependences of Thermal Conductivity of Porous Ceramic Materials: 2. Refractories and Ceramics with Porosity Exceeding 30%, *J. Am. Ceram. Soc.*, 1996, **79**, p 1366-1376
8. E.Y. Litovskii, On the Determinacy of Results Obtained in a Study of the Thermal Conductivity and Diffusivity of Ceramic Materials, *J. Eng. Phys.*, 1972, **22**, p 768-769
9. F. Cernuschi, P. Bison, and A. Moscatelli, Microstructural Characterization of Porous Thermal Barrier Coatings by Laser Flash Technique, *Acta Mater.*, 2009, **57**, p 3460-3471
10. I.O. Golosnoy, S.A. Tsipas, and T.W. Clyne, An Analytical Model for Simulation of Heat Flow in Plasma-Sprayed Thermal Barrier Coatings, *J. Therm. Spray Tech.*, 2005, **14**, p 205-214
11. S. Deshpande, A. Kulkarni, S. Sampath, and H. Herman, Application of Image Analysis for Characterization of Porosity in Thermal Spray Coatings and Correlation with Small Angle Neutron Scattering, *Surf. Coat. Technol.*, 2004, **187**, p 6-16
12. G. Antou, G. Montavon, F. Hlawka, A. Cornet, and C. Coddet, Characterizations of the Pore-Crack Network Architecture of Thermal-Sprayed Coatings, *Mater. Charact.*, 2004, **53**, p 361-372
13. S.A. Langer, E. Fuller, and W.C. Carter, OOF: An Image-Based Finite-Element Analysis of Material Microstructures, *Comput. Sci. Eng.*, 2001, **3**, p 15-23
14. A.C.E. Reid, S.A. Langer, R.C. Lua, V.R. Coffman, S.-I. Haan, and R.E. García, Image-Based Finite Element Mesh Construction for Material Microstructures, *Comput. Mater. Sci.*, 2008, **43**, p 989-999
15. K. Bakker and R.J.M. Konings, On the Thermal Conductivity of Inert-Matrix Fuels Containing Americium Oxide, *J. Nucl. Mater.*, 1998, **254**, p 129-134
16. W. Tillmann, B. Klusemann, J. Nebel, and B. Svendsen, Analysis of the Mechanical Properties of an Arc-Sprayed WC-FeCSiMn Coating: Nanoindentation and Simulation, *J. Therm. Spray Tech.*, 2010, **20**, p 328-335
17. B. Klusemann, R. Denzer, and B. Svendsen, Microstructure-Based Modeling of Residual Stresses in WC-12Co-Sprayed Coatings, *J. Therm. Spray Tech.*, 2011, **21**, p 96-107
18. R. Ghafouri-Azar, J. Mostaghimi, and S. Chandra, Modeling Development of Residual Stresses in Thermal Spray Coatings, *Comput. Mater. Sci.*, 2006, **35**, p 13-26
19. Z. Wang, A. Kulkarni, S. Deshpande, T. Nakamura, and H. Herman, Effects of Pores and Interfaces on Effective Properties of Plasma Sprayed Zirconia Coatings, *Acta Mater.*, 2003, **51**, p 5319-5334
20. A.D. Jadhav, N.P. Padture, E.H. Jordan, M. Gell, P. Miranzo, and E.R. Fuller, Low-Thermal-Conductivity Plasma-Sprayed Thermal Barrier Coatings with Engineered Microstructures, *Acta Mater.*, 2006, **54**, p 3343-3349
21. A. Kulkarni, J. Gutleber, S. Sampath, A. Goland, W.B. Lindquist, H. Herman, A.J. Allen, and B. Dowd, Studies of the Microstructure and Properties of Dense Ceramic Coatings Produced by High-Velocity Oxygen-Fuel Combustion Spraying, *Mater. Sci. Eng. A*, 2004, **369**, p 124-137
22. A. Kulkarni, A. Goland, H. Herman, A.J. Allen, T. Dobbins, F. DeCarlo, J. Ilavsky, G.G. Long, S. Fang, and P. Lawton, Advanced Neutron and X-Ray Techniques for Insights into the Microstructure of EB-PVD Thermal Barrier Coatings, *Mater. Sci. Eng. A*, 2006, **426**, p 43-52
23. A. Kulkarni, S. Sampath, A. Goland, H. Herman, and B. Dowd, Computed Microtomography Studies to Characterize Microstructure-Property Correlations in Thermal Sprayed Alumina Deposits, *Scripta Mater.*, 2000, **43**, p 471-476
24. T. Wiederkehr, B. Klusemann, D. Gies, H. Muller, and B. Svendsen, An Image Morphing Method for 3D Reconstruction and FE-Analysis of Pore Networks in Thermal Spray Coatings, *Comput. Mater. Sci.*, 2010, **47**, p 881-889
25. K. Bobzin, N. Kopp, T. Warda, and M. Öte, Determination of the Effective Properties of Thermal Spray Coatings Using 2D and 3D Models, *J. Therm. Spray Tech.*, 2012, **21**, p 1269-1277
26. R. Bolot, J.L. Seichepine, J.H. Qiao, and C. Coddet, Predicting the Thermal Conductivity of AlSi/Polyester Abradable Coatings: Effects of the Numerical Method, *J. Therm. Spray Tech.*, 2011, **20**, p 39-47
27. R. Bolot, G. Antou, G. Montavon, and C. Coddet, A Two-Dimensional Heat Transfer Model for Thermal Barrier Coating Average Thermal Conductivity Computation, *Numer. Heat Transf. A*, 2005, **47**, p 875-898
28. R. Bolot, J.H. Qiao, G. Bertrand, P. Bertrand, and C. Coddet, Effect of Thermal Treatment on the Effective Thermal Conductivity of YPSZ Coatings, *Surf. Coat. Technol.*, 2010, **205**, p 1034-1038
29. J.H. Qiao, R. Bolot, H. Liao, P. Bertrand, and C. Coddet, A 3D Finite-Difference Model for the Effective Thermal Conductivity of Thermal Barrier Coatings Produced by Plasma Spraying, *Int. J. Therm. Sci.*, 2013, **65**, p 120-126
30. H. Herman, Plasma-Sprayed Coatings, *Sci. Am.*, 1988, **259**, p 112-118
31. H. Singh and A.M. Gokhale, Visualization of Three-Dimensional Microstructures, *Mater. Charact.*, 2005, **54**, p 21-29
32. J.E. Spowart, Automated Serial Sectioning for 3-D Analysis of Microstructures, *Scripta Mater.*, 2006, **55**, p 5-10
33. J.H. Qiao, R. Bolot, and H. Liao, Finite Element Modeling of the Elastic Modulus of Thermal Barrier Coatings, *Surf. Coat. Technol.* (in press), 2012, doi:10.1016/j.surfcoat.2012.05.031

34. C. Vachiratienchai, S. Boonchaisuk, and W. Siripunvaraporn, A Hybrid Finite Difference-Finite Element Method to Incorporate Topography for 2D Direct Current (DC) Resistivity Modeling, *Phys. Earth Planet. Interiors*, 2010, **183**, p 426-434
35. G. Bertrand, P. Bertrand, P. Roy, C. Rio, and R. Mevrel, Low Conductivity Plasma Sprayed Thermal Barrier Coating Using Hollow PSZ Spheres: Correlation Between Thermophysical Properties and Microstructure, *Surf. Coat. Technol.*, 2008, **202**, p 1994-2001